ARTICLE

Excised linear introns regulate growth in yeast

Jeffrey T. Morgan[1,2,3], Gerald R. Fink[2,3] & David P. Bartel[1,2,3]*

Spliceosomal introns are ubiquitous non-coding RNAs that are typically destined for rapid debranching and degradation. Here we describe 34 excised introns in *Saccharomyces cerevisiae* that—despite being rapidly degraded in log-phase growth—accumulate as linear RNAs under either saturated-growth conditions or other stresses that cause prolonged inhibition of TORC1, which is a key integrator of growth signalling. Introns that become stabilized remain associated with components of the spliceosome and differ from other spliceosomal introns in having a short distance between their lariat branch point and 3′ splice site, which is necessary and sufficient for their stabilization. Deletion of these unusual introns is disadvantageous in saturated conditions and causes aberrantly high growth rates in yeast that are chronically challenged with the TORC1 inhibitor rapamycin. The reintroduction of native or engineered stable introns suppresses this aberrant rapamycin response. Thus, excised introns function within the TOR growth-signalling network of *S. cerevisiae* and, more generally, excised spliceosomal introns can have biological functions.

Spliceosomal introns are a defining feature of eukaryotic life; they are present in all known eukaryotic genomes and absent from all known non-eukaryotic genomes[1,2]. Introns and splicing can have important roles in eukaryotic gene evolution, mRNA expression and protein diversification[3]. Moreover, once excised from the primary transcript, introns can sometimes be further processed to generate non-coding RNAs, such as microRNAs or small nucleolar RNAs[4]. In principle, full-length excised introns could also be a fertile source of functional non-coding RNAs. However, excised intron lariats are debranched and degraded within seconds[5–9], and thus are generally viewed as inert and ephemeral by-products of gene expression[10].

Functions for individual introns have been examined most thoroughly in the intron-poor budding yeast *S. cerevisae*, which contains approximately 300 spliceosomal introns, with only a few annotated cases of alternative-splicing events[11–13]. For most introns tested, no growth phenotypes are detected upon their removal[14–16], but for a few, phenotypes are observed. Some functions inferred from these phenotypes, such as an influence on gene expression[17,18], manifest entirely during pre-mRNA production and processing, and thus before the introns exist as separate RNA molecules. Other functions, such as providing a source of small nucleolar RNAs, occur after splicing, although in these cases the flanking portions of the intron are still rapidly catabolized[19]. Thus, functional analyses in *S. cerevisiae* support the prevailing view that the collective fate of introns after splicing is solely to be debranched and at least partially degraded.

Although most yeast introns have now been individually assayed for function, relatively few experimental conditions have been explored. Most experiments assay cells during log-phase growth, which provides consistent measurements in a standardized system that is sensitized to detect differences in growth and metabolism. However, outside of the laboratory, yeast cells are unlikely to spend many consecutive generations rapidly dividing and more often face limiting nutrients or other stresses[20]. Accordingly, we set out to examine the gene regulation of *S. cerevisiae* outside of the context of log-phase growth.

Accumulation of excised, linear introns

We performed RNA sequencing (RNA-seq) on two *S. cerevisiae* samples: one taken from a culture in log-phase growth and the other from a saturated culture in which cell density was minimally increasing. For most intron-containing genes (exemplified by *ACT1*), very few intron-mapping RNA-seq reads were observed from either culture condition (Fig. 1a), as expected if introns were rapidly degraded after splicing. However, for a subset of genes (exemplified by *ECM33*), many intron-mapping reads were observed specifically from the saturated culture (Fig. 1b). Indeed, the higher density of reads for the *ECM33* intron compared to that for its exons suggested that in this growth condition the intron accumulated to much greater levels (tenfold) than did its corresponding mature mRNA.

Read coverage dropped abruptly at the 5′ and 3′ boundaries of the *ECM33* intron (Fig. 1b, Extended Data Fig. 1), which suggested accumulation of full-length intron. To examine whether our RNA-seq analysis was detecting the accumulation of excised introns of a defined size, we probed RNA blots for the inferred RNA species. Probes to the *ECM33* intron detected a single major species migrating at the position expected for the full-length intron (Fig. 1c). Likewise, a probe for *SAC6*, another intron inferred by RNA-seq to accumulate in saturated culture (Fig. 1d), detected an RNA of the size expected for the full-length excised intron (Fig. 1e). These introns that accumulate in saturated cultures are hereafter called 'stable introns'.

A known mechanism by which excised introns can be protected from degradation is by evading debranching and persisting as either lariat RNAs or circular derivatives in which the lariat tail is missing[8,21]. However, these nonlinear species have either branched RNA or a 2′–5′ phosphodiester linkage, which would impede reverse transcriptase[7,22] and thereby cause RNA-seq reads to be depleted in the region of the branch point—a pattern that we did not observe in the RNA-seq profiles (Fig. 1b, Extended Data Fig. 1). To test further whether *ECM33* intronic RNA accumulated as either a lariat RNA or its circular derivative, we collected RNA from yeast that lacked Dbr1 (the enzyme that is required to debranch intron lariats[8]) and compared the *ECM33* intronic RNA that accumulated in the *dbr1Δ* strain with RNA that

[1]Howard Hughes Medical Institute, Cambridge, MA, USA. [2]Whitehead Institute for Biomedical Research, Cambridge, MA, USA. [3]Department of Biology, Massachusetts Institute of Technology, Cambridge, MA, USA. *e-mail: dbartel@wi.mit.edu
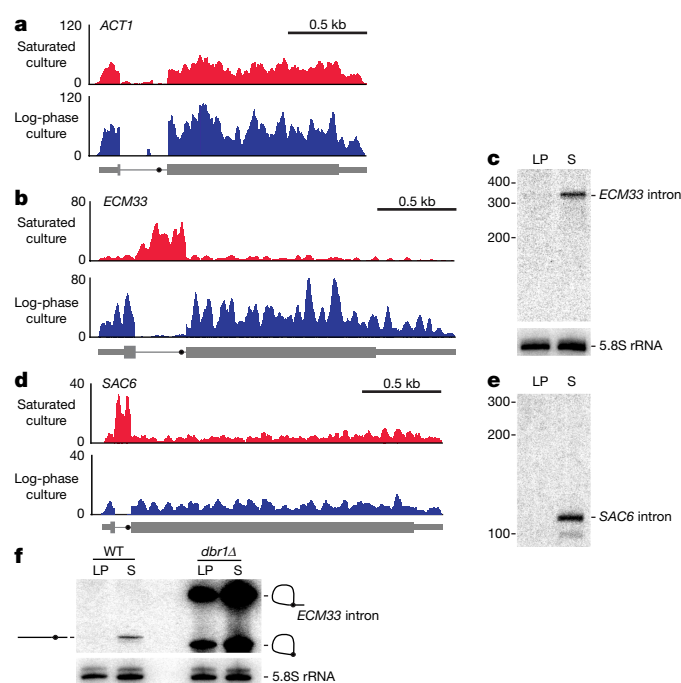
Fig. 1 | Some excised linear introns accumulate in yeast. a, Undetectable accumulation of the *ACT1* intron. RNA-seq profiles for *ACT1* are shown in both log-phase and saturated cultures. Thick box, coding sequence; thin box, untranslated region; line, intron; closed circle on intron, branch point. For each nucleotide of the locus, the number of reads per million combined exon- and intron-mapping reads of the library is plotted. $n = 2$ biological replicates. **b**, Accumulation of the *ECM33* intron in saturated but not log-phase culture, otherwise as in **a**. **c**, Accumulation of intact *ECM33* intron in saturated culture. An RNA blot that resolved total RNA from both log-phase (LP) and saturated (S) cultures and was probed for the *ECM33* intron is shown. Migration of markers with lengths indicated (nucleotides) is shown on the left. For a loading control, the blot was re-probed for 5.8S rRNA. $n = 12$ biological replicates. **d**, Accumulation of the *SAC6* intron in saturated but not log-phase culture, otherwise as in **a**. **e**, Intact *SAC6* intron detected by re-probing the RNA blot of **c**; otherwise, as in **c**. **f**, Accumulation of debranched *ECM33* intron in saturated culture. Analysis is as in **c**, except that the RNA blot included samples from both wild-type and *dbr1Δ* cultures. Migration of the linear isoform is indicated (diagram on the left) as is migration of both the lariat and the circular isoforms (diagrams on the right). $n = 3$ biological replicates.

accumulated in wild-type saturated cultures. As expected, in *dbr1Δ* cultures the *ECM33* intron was detected as two abundant species, which corresponded to the branched lariat and its circular derivative (Fig. 1f). Importantly, neither of these nonlinear species co-migrated with the linear intron identified in wild-type saturated cultures. These results confirmed that Dbr1 is necessary to form linear introns outside of log phase and showed that the previously known mode of decreased intron turnover cannot explain the accumulation of excised introns in a saturated culture.

Another mechanism that might protect stable introns from degradation in saturated cultures is incorporation into a ribonucleoprotein complex. Indeed, the *ECM33* intron predominantly co-sedimented with complexes that were about the size of ribosomal subunits (35–50 Svedberg units, Extended Data Fig. 2a). To identify proteins that associate with the intron, we performed pull-down experiments from gradient fractions that contained the intron and used quantitative mass spectrometry to identify co-purifying proteins. For these experiments, we took advantage of the observation that tagged versions of the *ECM33* intron excised from expression constructs retained the behaviour of the endogenous *ECM33* intron (Extended Data Fig. 2b, c). Each of the top 10 proteins that consistently co-purified with MS2-tagged versions of the *ECM33* intron (average enrichment, 4.9-fold) were spliceosomal proteins, the identities of which indicated that the excised

and debranched *ECM33* intron resided in a specific complex; when compared to known spliceosome complexes, this complex most closely resembled the intron–lariat spliceosome (ILS) complex[23] (Extended Data Table 1).

Studies in log-phase extracts indicate that introns are debranched after spliceosome disassembly[24]. If stable introns were also debranched outside the spliceosome, they would then need to re-associate with spliceosome components as linear RNAs. A simpler model is one of continued association of stable introns with ILS components during their debranching; in this case, the relationship between ILS disassembly and debranching presumably varies depending on growth condition and/or intron identity. In either scenario, our findings indicated that, in saturated cultures, accumulating introns are bound to and presumably protected by a complex that resembles the ILS.

Defining features of stable introns

We performed a systematic search for all introns that undergo a switch in stability and accumulate as linear RNAs in saturated cultures. In this search, RNA-seq reads of each intron-containing gene were analysed for a preponderance of reads that mapped to introns—particularly those that mapped to edges of excised introns (consistent with a post-splicing intron) relative to those that mapped across splice sites and splice junctions (which represented signatures of intron retention and mature mRNA expression, respectively)[25] (Extended Data Fig. 3a). Inspection of RNA-seq reads that mapped to 3′ edges of stable introns identified many that were extended by one or more untemplated adenosine residues (Extended Data Fig. 3b). Short 3′-terminal oligoadenylate tails are added by the TRAMP complex to mark nuclear RNAs for degradation[26,27]. Our finding that many stable-intron molecules had these tails suggested that these molecules might have been targeted for exosomal decay, yet had somehow escaped this decay. Regardless of their function, these untemplated adenosine residues provided an additional criterion for annotation of stable introns, which helped us to confidently identify another 28 introns that accumulated in saturated cultures (Extended Data Fig. 4, Extended Data Table 2).

We searched among the 30 stable introns for common features, which cellular machinery might use to differentiate them from the remaining introns that are rapidly degraded in saturated cultures. Compared to other introns, stable introns had similar strengths of canonical splicing motifs (Extended Data Fig. 5a), similar length distributions (Extended Data Fig. 5b), no common predicted structures or enriched sequence motifs (Extended Data Fig. 5c, d), and no enriched functional ontologies of their host genes. Of all the features we examined, the only one that differed was the distance between the lariat branch point and 3′ splice site (3′SS), which tended to be shorter for stable introns (Fig. 2a).

To investigate a potential role of branch-point position in influencing intron stability, we introduced mutations that changed endogenous branch point–3′SS distances and examined the effects on intron accumulation. Lengthening the short branch point–3′SS distance of the normally stable *ECM33* intron from 25 to 45 nucleotides abrogated the accumulation of the full-length excised intron, which indicated that a short branch point–3′SS distance is required for the stability of this intron (Fig. 2b). Moreover, shortening the branch point–3′SS distance of the normally unstable *ACT1* intron from 44 to 25 nucleotides conferred stability to this intron in saturated culture, which suggested that a short branch point–3′SS distance is not only necessary but also sufficient for stability (Fig. 2b).

The notion that a short branch point–3′SS distance is sufficient for stability suggested that introns that had short branch point–3′SS distances yet were not identified as stable introns (Fig. 2a) might not have been transcribed during the period at which stable introns are protected from degradation. To investigate this possibility, we used our expression construct to express introns that had not been identified as stable introns, choosing two introns with a short (20- and 25-nucleotide) and two with a long (37- and 44-nucleotide) branch point–3′SS distance. The two with short branch point–3′SS distances accumulated
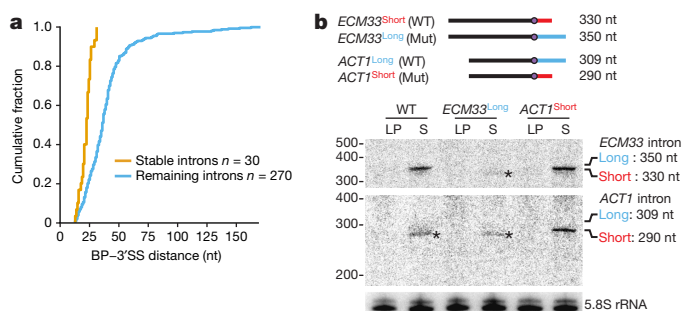
Fig. 2 | Stable introns have short branch point–3′SS distances.
a, Shorter branch point (BP)–3′SS distances of stable introns. Cumulative distributions of branch point–3′SS distances are plotted ($P = 1.3 \times 10^{-9}$, two-tailed Kolmogorov–Smirnov test). **b**, Causal relationship between branch point–3′SS distance and stable-intron formation. Top, wild-type (WT) and mutant (Mut) introns, in which the wild-type *ECM33* branch point–3′SS distance was extended from 25 nt ('short', red) to 45 nt ('long', blue), and the wild-type *ACT1* branch point–3′SS distance was shortened from 44 nt (long, blue) to 25 nt (short, red). Bottom, an RNA blot that resolved samples from the indicated strains and was probed sequentially for the *ECM33* intron (top), the *ACT1* intron (middle) and 5.8S rRNA (bottom). Probes were complementary to portions of introns that are common to both short and long isoforms. The expected migration of long and short linear isoforms of each intron is given on the right. The asterisks mark the detection of long-isoform degradation products, each of which migrated faster than did the short isoform. $n = 3$ biological replicates.

specifically in saturated cultures, whereas the two with long branch point–3′SS distances were unstable in both conditions (Extended Data Fig. 5e).

Thus, the two defining features of stable introns are (1) a short branch point–3′SS distance; and (2) expression within a cellular context in which introns are stabilized. After being modified to satisfy these criteria, all tested non-stable introns became stable introns (Fig. 2b, Extended Data Fig. 5e), which indicated that no other feature of either the intron or the host gene is required to achieve stability.

Regulation of stable introns
We next monitored levels of the *ECM33* stable intron and its host mRNA through 72 h of culture to determine when the switch in intron stability occurred (Fig. 3a). The *ECM33* mRNA levels were highest during rapid growth, whereas its intron levels were low through 8 h of growth and then markedly increased as cells exited rapid growth (Fig. 3a). Intron abundance remained high for at least the next 62 h, even as levels of mature mRNA decreased 23-fold. Although the dynamics of the *ECM33* intron and mRNA illustrated the different behaviours sometimes observed for stable introns and their host mRNAs, the large decrease in the levels of the mature mRNA in saturated culture was not observed for most mRNAs that hosted stable introns (Extended Data Fig. 5f).

The timing of stable-intron accumulation suggested that their formation might be linked to exit from rapid growth. With this in mind, we used rapamycin to inhibit the target of rapamycin complex 1 (TORC1), which is a broadly conserved master integrator of nutritional and other environmental signals[28,29]. In yeast, rapamycin-mediated TORC1 inhibition leads to repression of anabolic processes, stimulation of catabolic processes and greatly reduced growth[28]. When a log-phase culture was resuspended in fresh medium containing rapamycin, the *ECM33* intron accumulated after 4 h (Fig. 3b). A repeat of this experiment using a strain with a rapamycin-resistant allele of *TOR1* (*TOR1-1*) yielded no accelerated intron accumulation upon treatment with rapamycin (Fig. 3c). *TOR1-1* cultures nonetheless accumulated stable introns upon reaching saturation (Fig. 3c), as expected in this strain that is known to be sensitive to endogenous TORC1 inhibition[30]. Thus, rapamycin-induced intron accumulation was specifically due to inhibition of TORC1. The inhibition of protein synthesis in a TORC1-independent

manner did not cause stable-intron formation (Extended Data Fig. 6a). Moreover, stable introns accumulated to lower levels in the TORC1* strain, which contains six hyperactive alleles of the regulatory network[31] (Extended Data Fig. 7a)—results that further validated the involvement of TORC1 signalling.

To extend this investigation to the transcriptome, we prepared RNA-seq libraries from yeast that were treated for 4 h with rapamycin. We also investigated stable-intron formation in a metabolically different saturated-growth scenario: a lawn of yeast grown over 3 days in an aerobic environment. When compared to saturated-liquid culture, both rapamycin-treated cells and cells from the lawn showed a similar accumulation of not only the *ECM33* intron (Extended Data Fig. 7b) but also other stable introns (Extended Data Fig. 7c). In total, 34 introns (11% of total *S. cerevisiae* introns) were classified as stable introns in at least one of the three conditions (Extended Data Fig. 4, Extended Data Table 2).

We tested several genetic and environmental perturbations for their effects on stable-intron accumulation. Gain-of-function mutations in *TAP42* or *SCH9* (the two major effector branches of TORC1) were individually insufficient to override TORC1 repression and attenuate stable-intron formation (Extended Data Fig. 6b, c), and Sch9 activity was not required for stable-intron regulation (Extended Data Fig. 6d), which implicated involvement of another effector branch of TORC1. Although depletion of carbon, nitrogen and amino acids rapidly inhibit facets of TORC1 signalling[28], these conditions did not induce premature stable-intron formation (Extended Data Fig. 6e). Likewise, direct perturbations of the general amino acid control pathway did not disrupt stable-intron regulation (Extended Data Fig. 6f, g). Thus, the role of TORC1 in stable-intron regulation appeared separable from its role in rapid response to nutrient deprivation.

As illustrated for the *ECM33* intron (Fig. 3d), stable introns were not detected after treating with rapamycin for 1 h—a time period that is sufficient to phenocopy the TORC1 response to nutrient deprivation. This result was consistent with our observation that some conditions that are known to rapidly inhibit aspects of TORC1 signalling did not induce stable introns, and motivated an attempt to account for this delayed response to rapamycin. Few studies have explored prolonged TORC1 inhibition in yeast, and those that report on ≥2-h rapamycin treatments observe notably different TORC1-mediated responses compared to short-term rapamycin treatment or starvation[32–35]. Some of these studies[33–35] show that prolonged TORC1 inhibition (≥2-h treatment with rapamycin or tunicamycin) phenocopies secretory stress more closely than nutrient stress. We found that the secretory stressors tunicamycin and dithiothreitol (DTT) induced stable-intron formation, that for both stressors this induction required extended treatment durations similar to that required for rapamycin, and that induction of stable introns by these canonical activators of the unfolded-protein response did not require *IRE1*, the essential sensor of the unfolded-protein response (Fig. 3e, f). These results indicated that TORC1-mediated stable-intron accumulation depends on connections between TORC1 and membrane-trafficking or secretory stress[36,37], and not the more-often-considered connections between TORC1 and nutrient stress.

Biological function of stable introns
The discovery of stable introns and their link to the TORC1 growth-signalling pathway brought to the fore the question of their function. To build strains to test for loss-of-function phenotypes, we used a CRISPR–Cas9 system[38,39] that facilitated precise removal of introns without affecting exonic sequences. We reasoned that stable introns might contribute collectively to function, and therefore generated a quintuple mutant that lacked stable introns of five genes (*ECM33*, *UBC4*, *HNT1*, *SAC6* and *RFA2*). Because introns from these genes normally accumulated to high levels, this strain, which we call EUHSR, had less than half the stable intron molecules as compared to the wild-type strain (Fig. 4a, Extended Data Fig. 8a).

To detect the consequences of reducing stable-intron abundance, we co-cultured the EUHSR and wild-type strains in a competitive-growth
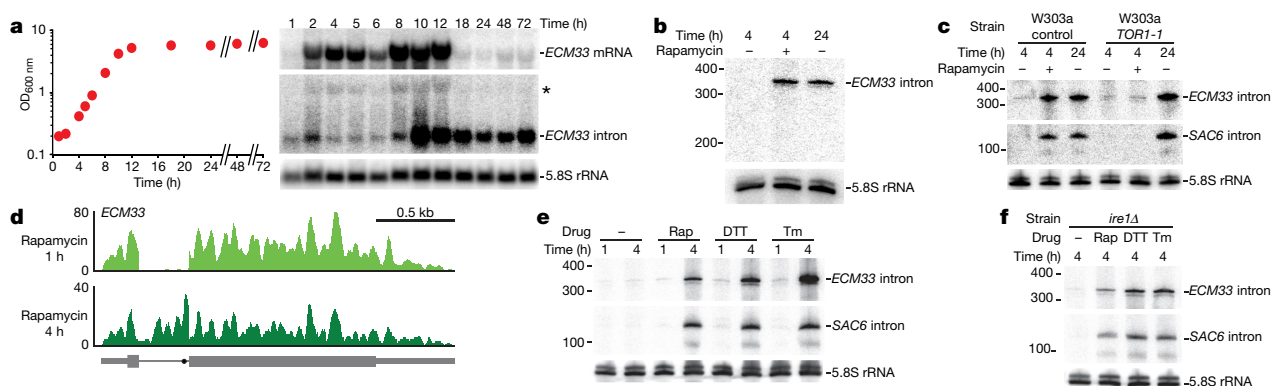
Fig. 3 | Stable-intron accumulation occurs after prolonged TORC1 inhibition. a, Distinct accumulation patterns of the *ECM33* stable intron and its host mRNA. After seeding at $OD_{600\,nm} = 0.2$, growth was monitored (left), and aliquots were collected for RNA-blot analysis (right). The blot is as in Fig. 1c, except it used a gel designed to resolve longer RNAs. The asterisk marks the migration of the *ECM33* pre-mRNA. **b**, Accumulation of the *ECM33* stable intron in cells cultured with rapamycin. Cultures were allowed to grow to early log phase, collected by vacuum filtration, resuspended in fresh medium with or without 100 nM rapamycin, collected at indicated times and analysed as in Fig. 1c. $n = 6$ biological replicates. **c**, Requirement of rapamycin-sensitive TORC1 for induction of stable introns by rapamycin. Results of a W303a control strain are compared to those of a W303a strain containing a rapamycin-

insensitive allele of *TOR1* (*TOR1-1*)[45]. Otherwise, this panel is as in **b**, except that the RNA blot was additionally re-probed for the *SAC6* intron. $n = 2$ biological replicates. **d**, Undetectable accumulation of the *ECM33* intron after 1 h of rapamycin treatment. Accumulation of this intron after 4 h of rapamycin treatment is shown for comparison. Otherwise, this panel is as in Fig. 1a. **e**, Accumulation of stable introns in cells cultured with 100 nM rapamycin (Rap), 5 mM dithiothreitol (DTT) or 1 μg ml^{-1} tunicamycin (Tm). Otherwise, this panel is as in **b**, except that the RNA blot was also probed for the *SAC6* intron. $n = 3$ biological replicates. **f**, Accumulation of stable introns in cells cultured with DTT or tunicamycin despite deletion of *IRE1*. Otherwise, this panel is as in **e**. $n = 2$ biological replicates.

assay. The co-culture was grown for three days, diluted, grown for three days again, and so on, for a total of six cycles of growth. Time points taken just before dilution and after a day of regrowth revealed a saw-tooth pattern in which the wild-type strain had a significant advantage during the period of sustained saturated culture, whereas EUHSR had a significant advantage during the period that included re-entry to growth and exit from growth (Fig. 4b). These results indicated that stable-intron expression is beneficial in some physiological contexts and detrimental in others.

Because of the connection between TORC1 inhibition and stable-intron formation (Fig. 3b–f), we tested the effect of rapamycin on growth of mutant strains from a series of intron deletions that produced decreasing amounts of stable introns (Fig. 4a). In contrast to the co-culture experiment (Fig. 4b), seeding was with log-phase cultures, which helped to explain why all strains grew at equivalent rates in the absence of rapamycin (Fig. 4c). In the presence of rapamycin, growth was inhibited for all strains, but this growth inhibition was attenuated for strains with fewer stable introns (Fig. 4c). A notable correlation was observed between the estimated fraction of stable-intron molecules depleted from the transcriptome and attenuation of the rapamycin response (Fig. 4c, d). By contrast, the rapamycin response of control strains that lacked non-stable introns of highly expressed genes was indistinguishable from that of wild type (Fig. 4d, inset), which showed that the observed phenotype was specific to depletion of stable introns and not merely a consequence of decreased splicing load.

The attenuated response to TORC1 inhibition seemed to depend solely on the number of stable-intron molecules removed from the cell, and not on the identities of either the removed introns or their host genes (Fig. 4d). This finding suggested that the phenotype did not result from subtle changes in host-gene expression or other secondary effects of intron removal or strain construction (such as off-target effects of gene editing). To test the conclusion that the attenuated response to TORC1 inhibition depended solely on the aggregate number of stable-intron molecules produced, we examined the ability of ectopically expressed introns to rescue the phenotype. We first overexpressed the *ECM33* stable intron or—as a control—its unstable derivative, which had a lengthened branch point–3′SS distance; these are referred to as *ECM33*-stable and *ECM33*-unstable, respectively. The stability of this overexpressed intron had no detectable effect on either wild-type or EUHSR growth in the absence of rapamycin, and had little effect on

growth of the wild-type strain in rapamycin (Fig. 4e). Importantly, however, the stability of this ectopically expressed intron markedly influenced the growth of the quintuple mutant in the presence of rapamycin—nearly completely rescuing its defective response to rapamycin (Fig. 4e). Analogous results were observed when using stabilized and normal versions of the *ACT1* intron (referred to as *ACT1*-stable and *ACT1*-unstable, respectively) (Fig. 4f). The ability of a stable version of the *ACT1* intron (which does not exist naturally in *S. cerevisiae*) to rescue the quintuple-mutant phenotype confirmed that this phenotype was a primary consequence of reduced stable-intron abundance.

Taken together, our results show that stable introns function within the TORC1-mediated stress response in *S. cerevisiae* (Fig. 4g). TORC1 activity prevents stable-intron formation, as shown by the accumulation of these introns when cells undergo prolonged TORC1 inhibition (Fig. 3b–f), and stable introns inhibit growth of cells with decreased TORC1 activity, as shown by the increased growth observed in TORC1-inhibited strains with fewer stable introns (Fig. 4c–f). Thus, this double-negative regulation—in which TORC1 inhibits stable introns, which in turn inhibit growth—forms a previously unknown node of the TOR regulatory network, which works in concert with other TORC1-dependent and TORC1-independent pathways to control growth in *S. cerevisiae* (Fig. 4g).

Mechanistic possibilities

The discovery of this node of the TOR regulatory network raises mechanistic questions, including that of how stable-intron accumulation might inhibit growth. Our results imply that the stoichiometry of stable introns relative to some cellular component underlies this function. One possibility is that stable introns sequester spliceosomes to reduce splicing activity. Supporting this idea, stable introns associate with spliceosome components (Extended Data Table 1) and *S. cerevisiae* pre-mRNAs compete for limited splicing machinery[40]. Moreover, in budding yeast sequestering spliceosomes might disproportionately affect mRNAs of ribosomal protein genes; because of their high expression levels and frequent possession of an intron, mRNAs of ribosomal protein genes are substrates for 90% of all splicing events in log-phase *S. cerevisiae*[41]. Although this percentage presumably decreases as cells exit log phase, stable introns could function as part of a larger regulatory network that uses inefficient splicing to help to keep ribosome production low during prolonged environmental and intracellular insults[41,42].

Fig. 4 | Stable introns influence yeast fitness and growth. a, Stable-intron genomic deletions and their estimated effect on total stable-intron molecules. Strains were named using single-letter abbreviations of genes with deleted introns (shown in colour key). **b**, Altered fitness of the EUHSR strain. Left, co-cultures of wild type and EUHSR were diluted every three days (dashed lines). The fraction of wild type in each co-culture, measured before each dilution and a day after each dilution, is plotted. Lines for each biological replicate are coloured to indicate periods of saturated growth (blue), returning to and exiting rapid growth (orange), and initial post-seeding (black). Right, mean fold change of wild type (expressed as $\log_2$ (fraction of wild type at earlier time point/fraction of WT at later time point)) during periods of saturated growth (blue, $n = 10$, $P = 9.4 \times 10^{-5}$, 95% confidence interval 0.12 to 0.25, two-tailed t-test) and return to and exit from rapid growth (orange, $n = 12$, $P = 1.0 \times 10^{-6}$, 95% confidence interval -0.74 to -0.46, two-tailed t-test). Error bars, s.e.m; **$P < 1 \times 10^{-4}$. **c**, Attenuated rapamycin response of strains with fewer stable-intron molecules. Curves show growth of wild-type and deletion strains in either 0, 100 or 250 nM rapamycin. **d**, Relationship between depletion of stable-intron molecules (given in **a**) and increased growth in 250 nM rapamycin. Inset, control strains in which 1–3 unstable introns were deleted. Control strains named as in **a**. $n = 12$ biological replicates for wild type, $n = 3$ for other strains; error bars, s.e.m. **e**, Rescue of the rapamycin-response defect by the *ECM33* intron. Curves show growth of wild-type and EUHSR strains that overexpress either the native (red) or unstable (blue) *ECM33* intron cultured in either 0 or 250 nM rapamycin. $n = 3$ biological replicates. **f**, Rescue by an engineered *ACT1* stable intron. As in **e**, but expressing either the native (blue) or stable (red) *ACT1* intron. **g**, Stable introns (coloured lines) in the TORC1 network.

To evaluate this idea, we revisited our RNA-seq data from rapamycin-treated yeast with the goal of determining the aggregate level of stable introns relative to spliceosome components. This analysis showed that stable-intron molecules reached 40% of the level of U5 small nuclear RNA molecules (Extended Data Fig. 8b), and in principle, an essential splicing protein could be more limiting than this small nuclear RNA. Thus, stable-intron accumulation was within a regime in which depleting 55% of stable-intron molecules—as in our EUHSR strain—could substantially alter spliceosome availability. Furthermore, overexpressing a stable intron (*ECM33*) in the EUHSR strain grown in rapamycin resulted in more intron retention and less accumulation of mRNAs of ribosomal protein genes as compared with overexpression of a non-stable intron (*ACT1*) (Extended Data Fig. 8c, d). Future

characterization of the stable-intron complex will provide more-detailed information on the cellular machinery that is sequestered and might also provide insight into other mechanistic questions, such as how stable introns are protected from degradation and how this protection is biochemically coupled to TORC1 inhibition.

Discussion

The ease with which we were able to observe the accumulation of stable introns raises the question of why they were not detected earlier. The answer lies with two features of our analysis. First, we examined cells in saturated culture, whereas most analyses examine cells in log phase—a stage at which all excised introns are rapidly degraded. Second, we avoided mRNA poly(A) selection, whereas many analyses perform poly(A) selection before RNA-seq; this selection depletes excised introns, which lack poly(A) tails. In addition, we used an in-house RNA-seq protocol in which RNA was fragmented, and fragments of 27- to 40-nucleotides in size were isolated for sequencing; by contrast, most analyses use commercial RNA-seq kits that deplete RNAs that are shorter than a few hundred nucleotides in size—the size of excised yeast introns. In principle, studies that used splicing-isoform microarrays to assay intron retention during stress, including rapamycin and DTT treatment, might have detected stable introns[40,43,44]. However, those studies focus on measurements over the course of 40 min, with no measurements taken beyond 2 h of treatment, which might not have been enough time to detect stable introns under these conditions. Our findings on prolonged TORC1 inhibition strengthen the links between TORC1 signalling and secretory stress in yeast[33–35], and show that short versus long durations of TORC1 inhibition can result in distinct effects on some downstream biological processes—including stable-intron regulation.

Although our ideas regarding the mechanism of stable-intron function require validation, one interesting aspect of this mechanism is that it operates regardless of stable-intron sequence or genomic origin. This observation provides an example in which the history of a non-coding RNA (that is, how the molecule is born) can be sufficient to impart a cellular function—independently of any primary-sequence considerations. Similar principles might apply to other non-coding RNAs, especially those that lack primary-sequence conservation.

Our results add to the known fates and functions of spliceosomal introns within eukaryotic biology. Although noteworthy examples of intron lariats and trimmed linear introns with lives after splicing have previously been reported[10], the introns described here are unique in that they persist as excised, full-length and debranched RNAs. Moreover, their stability is regulated in response to environmental changes, and they collectively act as a type of functional non-coding RNA. Our focus has been on the contexts of TORC1 inhibition and saturated growth, but stable introns might also be induced and have similar functions in other conditions. Although intron-rich eukaryotes cannot as obviously leverage spliceosome availability to manipulate the production of specific subsets of proteins, some might use excised linear introns to perform biological functions—perhaps in environmental conditions that have not yet been extensively profiled. At this point, we know that excised linear introns accumulate and function in at least one eukaryotic lineage, and we would be surprised if this is the only one.

Online content

Any methods, additional references, Nature Research reporting summaries, source data, statements of data availability and associated accession codes are available at https://doi.org/10.1038/s41586-018-0828-1.

1. Koonin, E. V. The origin of introns and their role in eukaryogenesis: a compromise solution to the introns-early versus introns-late debate? *Biol. Direct* **1**, 22 (2006).
2. Irimia, M. & Roy, S. W. Origin of spliceosomal introns and alternative splicing. *Cold Spring Harb. Perspect. Biol.* **6**, a016071 (2014).

3. Nilsen, T. W. & Graveley, B. R. Expansion of the eukaryotic proteome by alternative splicing. *Nature* **463**, 457–463 (2010).
4. Cech, T. R. & Steitz, J. A. The noncoding RNA revolution–trashing old rules to forge new ones. *Cell* **157**, 77–94 (2014).
5. Grabowski, P. J., Padgett, R. A. & Sharp, P. A. Messenger RNA splicing *in vitro*: an excised intervening sequence and a potential intermediate. *Cell* **37**, 415–427 (1984).
6. Padgett, R. A., Konarska, M. M., Grabowski, P. J., Hardy, S. F. & Sharp, P. A. Lariat RNA's as intermediates and products in the splicing of messenger RNA precursors. *Science* **225**, 898–903 (1984).
7. Ruskin, B., Krainer, A. R., Maniatis, T. & Green, M. R. Excision of an intact intron as a novel lariat structure during pre-mRNA splicing *in vitro*. *Cell* **38**, 317–331 (1984).
8. Chapman, K. B. & Boeke, J. D. Isolation and characterization of the gene encoding yeast debranching enzyme. *Cell* **65**, 483–492 (1991).
9. Pai, A. A. et al. The kinetics of pre-mRNA splicing in the *Drosophila* genome and the influence of gene architecture. *eLife* **6**, e32537 (2017).
10. Hesselberth, J. R. Lives that introns lead after splicing. *Wiley Interdiscip. Rev. RNA* **4**, 677–691 (2013).
11. Spingola, M., Grate, L., Haussler, D. & Ares, M., Jr. Genome-wide bioinformatic and molecular analysis of introns in *Saccharomyces cerevisiae*. *RNA* **5**, 221–234 (1999).
12. Davis, C. A., Grate, L., Spingola, M. & Ares, M., Jr. Test of intron predictions reveals novel splice sites, alternatively spliced mRNAs and new introns in meiotically regulated genes of yeast. *Nucleic Acids Res.* **28**, 1700–1706 (2000).
13. Juneau, K., Palm, C., Miranda, M. & Davis, R. W. High-density yeast-tiling array reveals previously undiscovered introns and extensive regulation of meiotic splicing. *Proc. Natl Acad. Sci. USA* **104**, 1522–1527 (2007).
14. Ng, R., Domdey, H., Larson, G., Rossi, J. J. & Abelson, J. A test for intron function in the yeast actin gene. *Nature* **314**, 183–184 (1985).
15. Parenteau, J. et al. Deletion of many yeast introns reveals a minority of genes that require splicing for function. *Mol. Biol. Cell* **19**, 1932–1941 (2008).
16. Hooks, K. B., Naseeb, S., Parker, S., Griffiths-Jones, S. & Delneri, D. Novel intronic RNA structures contribute to maintenance of phenotype in *Saccharomyces cerevisiae*. *Genetics* **203**, 1469–1481 (2016).
17. Parenteau, J. et al. Introns within ribosomal protein genes regulate the production and function of yeast ribosomes. *Cell* **147**, 320–331 (2011).
18. Bonnet, A. et al. Introns protect eukaryotic genomes from transcription-associated genetic instability. *Mol. Cell* **67**, 608–621.e606 (2017).
19. Petfalski, E., Dandekar, T., Henry, Y. & Tollervey, D. Processing of the precursors to small nucleolar RNAs and rRNAs requires common components. *Mol. Cell. Biol.* **18**, 1181–1189 (1998).
20. Gray, J. V. et al. "Sleeping beauty": quiescence in *Saccharomyces cerevisiae*. *Microbiol. Mol. Biol. Rev.* **68**, 187–206 (2004).
21. Wu, T.-T., Su, Y.-H., Block, T. M. & Taylor, J. M. Evidence that two latency-associated transcripts of herpes simplex virus type 1 are nonlinear. *J. Virol.* **70**, 5962–5967 (1996).
22. Lorsch, J. R., Bartel, D. P. & Szostak, J. W. Reverse transcriptase reads through a 2′-5′ linkage and a 2′-thiophosphate in a template. *Nucleic Acids Res.* **23**, 2811–2814 (1995).
23. Fourmann, J. B. et al. Dissection of the factor requirements for spliceosome disassembly and the elucidation of its dissociation products using a purified splicing system. *Genes Dev.* **27**, 413–428 (2013).
24. Martin, A., Schneider, S. & Schwer, B. Prp43 is an essential RNA-dependent ATPase required for release of lariat-intron from the spliceosome. *J. Biol. Chem.* **277**, 17743–17750 (2002).
25. Katz, Y., Wang, E. T., Airoldi, E. M. & Burge, C. B. Analysis and design of RNA sequencing experiments for identifying isoform regulation. *Nat. Methods* **7**, 1009–1015 (2010).
26. LaCava, J. et al. RNA degradation by the exosome is promoted by a nuclear polyadenylation complex. *Cell* **121**, 713–724 (2005).
27. Qin, D., Huang, L., Wlodaver, A., Andrade, J. & Staley, J. P. Sequencing of lariat termini in *S. cerevisiae* reveals 5′ splice sites, branch points, and novel splicing events. *RNA* **22**, 237–253 (2016).
28. Wullschleger, S., Loewith, R. & Hall, M. N. TOR signaling in growth and metabolism. *Cell* **124**, 471–484 (2006).
29. Saxton, R. A. & Sabatini, D. M. mTOR signaling in growth, metabolism, and disease. *Cell* **168**, 960–976 (2017).
30. Jorgensen, P. et al. A dynamic transcriptional network communicates growth potential to ribosome synthesis and critical cell size. *Genes Dev.* **18**, 2491–2505 (2004).
31. Goranov, A. I. et al. Changes in cell morphology are coordinated with cell growth through the TORC1 pathway. *Curr. Biol.* **23**, 1269–1279 (2013).
32. Zaragoza, D., Ghavidel, A., Heitman, J. & Schultz, M. C. Rapamycin induces the G_0 program of transcriptional repression in yeast by interfering with the TOR signaling pathway. *Mol. Cell. Biol.* **18**, 4463–4470 (1998).
33. Lempiäinen, H. et al. Sfp1 interaction with TORC1 and Mrs6 reveals feedback regulation on TOR signaling. *Mol. Cell* **33**, 704–716 (2009).
34. Mülleder, M. et al. Functional metabolomics describes the yeast biosynthetic regulome. *Cell* **167**, 553–565.e12 (2016).
35. Rousseau, A. & Bertolotti, A. An evolutionarily conserved pathway controls proteasome homeostasis. *Nature* **536**, 184–189 (2016).
36. Aronova, S., Wedaman, K., Anderson, S., Yates, J., III & Powers, T. Probing the membrane environment of the TOR kinases reveals functional interactions between TORC1, actin, and membrane trafficking in *Saccharomyces cerevisiae*. *Mol. Biol. Cell* **18**, 2779–2794 (2007).
37. Zurita-Martinez, S. A., Puria, R., Pan, X., Boeke, J. D. & Cardenas, M. E. Efficient Tor signaling requires a functional class C Vps protein complex in *Saccharomyces cerevisiae*. *Genetics* **176**, 2139–2150 (2007).
38. Vyas, V. K., Barrasa, M. I. & Fink, G. R. A *Candida albicans* CRISPR system permits genetic engineering of essential genes and gene families. *Sci. Adv.* **1**, e1500248 (2015).
39. Vyas, V. K. et al. New CRISPR mutagenesis strategies reveal variation in repair mechanisms among fungi. *MSphere* **3**, e00154-18 (2018).
40. Munding, E. M., Shiue, L., Katzman, S., Donohue, J. P. & Ares, M. Jr. Competition between pre-mRNAs for the splicing machinery drives global regulation of splicing. *Mol. Cell* **51**, 338–348 (2013).
41. Warner, J. R. The economics of ribosome biosynthesis in yeast. *Trends Biochem. Sci.* **24**, 437–440 (1999).
42. Gasch, A. P. et al. Genomic expression programs in the response of yeast cells to environmental changes. *Mol. Biol. Cell* **11**, 4241–4257 (2000).
43. Pleiss, J. A., Whitworth, G. B., Bergkessel, M. & Guthrie, C. Rapid, transcript-specific changes in splicing in response to environmental stress. *Mol. Cell* **27**, 928–937 (2007).
44. Bergkessel, M., Whitworth, G. B. & Guthrie, C. Diverse environmental stresses elicit distinct responses at the level of pre-mRNA processing in yeast. *RNA* **17**, 1461–1478 (2011).
45. Zheng, X.-F., Florentino, D., Chen, J., Crabtree, G. R. & Schreiber, S. L. TOR kinase domains are required for two distinct functions, only one of which is inhibited by rapamycin. *Cell* **82**, 121–130 (1995).

Author contributions Apart from tetrad dissections, which were performed by G.R.F., J.T.M. performed all experiments and analyses. D.P.B. supervised with help from G.R.F. All authors contributed to study design and manuscript preparation.

Competing interests The authors declare no competing interests.

Additional information
Extended data is available for this paper at https://doi.org/10.1038/s41586-018-0828-1.
Supplementary information is available for this paper at https://doi.org/10.1038/s41586-018-0828-1.
Reprints and permissions information is available at http://www.nature.com/reprints.
Correspondence and requests for materials should be addressed to D.P.B.
Publisher's note: Springer Nature remains neutral with regard to jurisdictional claims in published maps and institutional affiliations.

METHODS

Yeast strains and genetic manipulations. *S. cerevisiae* strains used in this study are listed in Supplementary Table 1. With the exception of strains acquired for *TOR1-1* (Fig. 3c) and TORC1* (Extended Data Fig. 7a) experiments, all strains were in the BY4741 background. A *TAP42* heterozygous diploid knockout strain (Horizon Discovery) was transformed with plasmids encoding either wild-type (*TAP42*) or mutant (*tap42-11*) alleles before sporulation and tetrad dissection. Transformations were performed using standard methods. Intron deletions and endogenous branch-point manipulations were made using a CRISPR–Cas9 system adapted for use in *S. cerevisiae*[38,39] and were confirmed by colony PCR and Sanger sequencing of relevant genomic loci. Clones with correct deletions were counter-selected for the Cas9 plasmid by plating onto 5-fluoroorotic acid (5-FOA) medium before their use in experiments. This process was iterated to generate strains with multiple deleted introns. Strains that underwent 5-FOA counter-selection were confirmed to not be petite by patching to YP-glycerol plates. *his3Δ1* repair was performed by transforming BY4741 with linear *HIS3* DNA, selecting for His+ transformants, and confirming repair of the endogenous locus by colony PCR and Sanger sequencing. Plasmids used in this study are listed in Supplementary Table 2. Oligonucleotides (IDT) used for guide RNAs and repair templates are listed in Supplementary Table 3.

Growth conditions and collecting. Yeast were grown at 30 °C on standard synthetic complete (SC) plate and liquid medium, except experiments involving TORC1* strains (Extended Data Fig. 7a), which were performed according to previously described protocols[31], and *tap42::KanMX* strains (Extended Data Fig. 6b), which were performed at 25 °C owing to temperature sensitivity. SC–Ura and SC–Trp were used in some experiments to maintain selection for *URA3-* and *TRP1*-expressing plasmids. SC–His was used in experiments involving 3-aminotriazole. Rapamycin (LC Laboratories; 10 mM stock in DMSO) aliquots were stored at −80 °C, and diluted to 10 μM in water immediately before use. 3-aminotriazole (Sigma-Aldrich; 1 M stock in water), cycloheximide (Sigma-Aldrich; 100 mg ml^{-1} stock in DMSO), DTT (Thermo Scientific; 1 M stock in water), and tunicamycin (Millipore-Sigma; 10 mg ml^{-1} stock in DMSO) aliquots were stored at −20 °C. Cultures were seeded at $OD_{600 \, nm}$ of 0.2 from overnight cultures (typically $OD_{600 \, nm}$ ∼6) for growth to log phase or saturation. Log-phase cultures were collected during early log phase, typically at $OD_{600 \, nm}$ of 0.5, reached 4–5 h after seeding. Unless otherwise indicated, saturated cultures were collected 18–20 h after seeding. In acute nutrient-depletion experiments, cultures were grown to mid-log phase ($OD_{600 \, nm}$ ∼1), filtered, washed twice with water and resuspended in appropriate medium (SC–glucose, SC–ammonium sulfate, SC–leucine or SC–uracil). All cultures were rapidly collected by vacuum filtration and flash-frozen in liquid nitrogen as described[46]. Frozen pellets were mechanically lysed using a Sample Prep 6870 Freezer/Mill (Spex SamplePrep; 10 cycles of 2 min on, 2 min off at setting 10). Lysate powder was aliquoted and stored at −80 °C.

Competitive growth. Wild-type and EUHSR strains were co-cultured in a series of batch cultures, which were performed in biological replicate. The experiment started with a 50-ml co-culture in a 250-ml baffled flask seeded with an equal amount of the two strains at a combined $OD_{600 \, nm}$ of 0.2. The co-culture was then allowed to grow to confluence for 3 days. At this point, it was diluted to $OD_{600 \, nm}$ of 0.2, and growth and dilution were repeated for a total of 6 cycles. Two 1-ml samples were taken at each cycle, one immediately before dilution and the other 24 h after dilution. Genomic DNA was collected using the "Bust 'n Grab" protocol[47], and the relative abundance of wild type and EUHSR was measured by PCR across the *ECM33* and *UBC4* intron-deletion loci (primers listed in Supplementary Table 3). By comparing to a standard curve of PCR results that had been templated with defined ratios of independently isolated wild-type and EUHSR genomic DNA (ranging from 1:4 to 4:1), the fractional content of wild-type cells was determined at each time point.

RNA-seq. Total RNA was extracted from lysate powder using TRI Reagent (Ambion) according to the manufacturer's protocol. rRNA was depleted from 5 μg of total RNA using the Ribo-Zero Gold Yeast rRNA Removal Kit (Illumina) according to the manufacturer's protocol. RNA-seq libraries were prepared as described[48] and sequenced on the Illumina HiSeq platform using 40-bp single reads. A detailed protocol is available at http://bartellab.wi.mit.edu/protocols.html.

RNA-seq analyses. Reads were trimmed of adaptor sequence using cutadapt (v.1.8)[49]. Trimmed reads were aligned to the *S. cerevisiae* genome (R64-1-1, downloaded from www.yeastgenome.org) using STAR (v.2.4)[50] with the parameters '–alignIntronMax 1000 –sjdbOverhang 31 –outSAMtype BAM SortedByCoordinate –quantMode GeneCounts' and with '–sjdbGTFfile' supplied with transcript annotations. Intron annotations were constructed from the UCSC Genome browser and the Ares laboratory yeast intron database (http://intron.ucsc.edu/yeast4.3/), with the Ares laboratory database[11,12] providing branch-point annotations used in subsequent analyses. RNA-seq visualization was performed using IGV (v.2.3.57)[51,52]. If multiple biological replicates were sequenced, figures show representative RNA-seq profiles from one of the replicates.

Untemplated nucleotides were found and catalogued by extracting reads from BAM files that uniquely mapped to the sense strand of an intron, but which also contained soft-clipped, non-mapping nucleotides at the 3′ end of the read. The mixture-of-isoforms (MISO, v.0.5.4)[25] framework was used to quantify the relative expression of three potential isoforms for every intron: spliced (intron-degraded), spliced (intron-stable) and intron retained. MISO requires uniform read length as input. As such, the 3′ adaptor sequence was removed by trimming a constant 8 nt from every read. Based on the distribution of prior cutadapt-mediated trimming, this removed all 3′ adaptor sequence from >98% of reads. Retained-intron GFF events were constructed using 'gff_make_annotation' from rnaseqlib (http://rnaseqlib.readthedocs.io/en/clip/). Stable-intron GFF events were made by directly modifying the retained-intron GFF events to instead include 'intron only' as a potential outcome of splicing. Although reads that supported a stable-intron splicing event necessarily could also support a retained-intron splicing event, in practice, the greater abundance of most stable introns relative to flanking exons enabled MISO to identify stable introns as the predominant isoform for many introns in stable-intron-inducing conditions.

To be identified as a stable intron expressed in a given condition, accumulation of the intron had to exceed thresholds calibrated on experimentally validated cases. First, intron accumulation (transcripts per million, TPM) in the stable-intron-inducing condition had to be greater than half of its associated mRNA accumulation (TPM). Second, the intron accumulation (TPM) in the stable-intron-inducing condition had to be more than twice that of its accumulation (TPM) in log phase (a pseudocount of 0.01 TPM was added to all introns to account for introns with zero mapped reads). Third, the ratio of intron:mRNA accumulation in the stable-intron-inducing condition had to be greater than fourfold that of the intron:mRNA ratio in log phase. Imposing these thresholds eliminated many false positives, including some attributed to intronic small nucleolar RNA expression or constitutively poor splicing. Additionally, all introns containing small nucleolar RNA were manually inspected for evidence of full-length introns, which was not found in any case. For introns exceeding these accumulation thresholds, at least one of the following two additional criteria were required for annotation as a stable intron: (1) ≥2 terminal adenylylated reads mapping to the 3′ terminus of the intron, and/or (2) MISO-based support for preferential accumulation of the stable-intron isoform in the stable-intron-inducing condition (Bayes factor ≥30 when compared to log phase). These criteria identified conservative sets of stable introns expressed in a given condition, erring towards reducing false-positive identifications.

A search for motifs enriched in stable introns was performed using the MEME suite[53] with remaining introns as the background set. *k*-mer frequencies were generated with the fasta-get-markov program from the MEME Suite. In addition, a search for enrichment of position-specific motifs was performed using *k*pLogo[54] with remaining introns as the background set.

Growth curves. Growth curves were collected using Nunc Edge 2.0 96-well plates in a Multiskan GO Microplate Spectrophotometer. Wells were seeded at $OD_{600 \, nm}$ = 0.2 from early-log-phase cultures, and plates were incubated at 30 °C. Absorbance was read every 5 min with shaking on the 'background' setting, cycling between 1 min on and 1 min off. Every strain tested on each plate was run in technical triplicate. Single wells were censored if artefactual spikes in $OD_{600 \, nm}$ attributable to bubbles or condensation were observed. Strains were censored if more than one well was censored. Biological replicates for each strain included at least two independently derived transformants. A replicate of parental BY4741 was included on every plate as a control strain, and SC medium was included on every plate as a control condition for every strain being assayed. The growth rate was calculated from the log-linear portion of each growth curve. Growth curves were analysed with SkanIt (v.3.2).

RNA blots. Total RNA was extracted from lysate powder using TRI Reagent (Ambion) according to the manufacturer's protocol. Ten micrograms of total RNA for each sample was resolved on a denaturing polyacrylamide gel and transferred onto a Hybond membrane (GE Healthcare) using a semi-dry transfer cell. Because ultraviolet crosslinking is biased against shorter RNAs, EDC (*N*-(3-dimethylaminopropyl)-*N*′-ethylcarbodiimide; Sigma-Aldrich) was used to chemically crosslink 5′ phosphates to the membrane[55]. Blots were hybridized to radio-labelled DNA probes. Probe oligonucleotides are listed in Supplementary Table 4. More details of this protocol are available at http://bartellab.wi.mit.edu/protocols.html. For experiments in Fig. 3a, RNAs were instead resolved on a glyoxal agarose gel and transferred overnight onto a Nytran SuPerCharge Turboblotter membrane (GE Healthcare). RNA-blot data were analysed with ImageQuant TL (v.8.1.0.0).

Sedimentation velocity. Crude lysates were prepared by resuspending an aliquot of thawed lysate powder (500–800 μl of loosely packed powder) in 1 ml of lysis buffer (10 mM Tris-HCl (pH 7.4), 5 mM $MgCl_2$, 100 mM KCl, 1% Triton X-100, 1% sodium deoxycholate, 2 mM DTT, 20 U/ml SUPERase•In (Ambion), and cOmplete EDTA-free Protease Inhibitor Cocktail (Roche)). The lysates were placed on a rotator mixer at 4 °C for 5 min to allow for resuspension. Following brief vortexing,

lysates were centrifuged at 1,300*g* for 10 min, and the supernatant loaded onto a 12.5-ml linear 10–30% (w/v) sucrose gradient (20 mM HEPES-KOH (pH 7.4), 5 mM MgCl$_2$, 100 mM KCl, 2 mM DTT, and 20 U/ml SUPERase•In). Gradients were centrifuged in a pre-chilled SW-41 Ti rotor at 38,000 rpm for 4 h at 4 °C. Gradients were fractionated using a Piston Gradient Fractionator (Biocomp) in 1-ml fractions. For RNA analysis, total RNA was extracted from a portion of each fraction using TRI Reagent. RNA blots were performed as described for total RNA, except RNA loading was normalized by per cent of gradient fraction rather than by RNA concentration. For pull-downs, fractions were flash-frozen and stored at −80 °C.

Ectopic intron expression, affinity purification and mass spectrometry. Intron-overexpression constructs were based on SC–Ura-selectable pRSII416 (CEN) or pRSII426 (2μ) vectors[56] (Extended Data Fig. 3c, Supplementary Table 2). Introns were inserted 49 nucleotides downstream of the *URA3* start codon by Gibson assembly. Proper splicing was confirmed by RNA blot and cell viability, as cells unable to produce Ura3p through intron removal could not grow on SC–Ura medium.

Pull-down experiments were performed in the *ECM33Δintron* strain. Introns were purified using two MS2 hairpins (2 × MS2) inserted in various positions within the *ECM33* intron (Supplementary Table 5). To minimize potential effects on splicing, the sequence within 60 nt of the 5′ splice site and 80 nt of the branch point was kept constant across all constructs. The 2 × MS2 hairpin sequence was based on CRISPR RNA scaffold designs[57]. 3×Flag-tagged MS2 coat protein with a C-terminal nuclear-localization signal (FLAG–MCP) was co-expressed from the constructs that also expressed the MS2-tagged introns.

We were unable to purify intact introns from the supernatant of saturated cultures owing to increased endogenous RNase activity in saturated cultures[58]. To circumvent this, sucrose-gradient fractions containing the intron of interest (typically fractions 6–9, determined by RNA blot) were pooled and used as the starting material for purification. Anti-Flag M2 Magnetic Beads (Sigma-Aldrich) (20 μl of packed-bead volume) were equilibrated and washed twice in 10 volumes of buffer 1 (100 mM KCl, 20 mM HEPES KOH (pH 7.9), 1% Triton X-100, 20 U/ml SUPERase•In, and cOmplete EDTA-free Protease Inhibitor Cocktail). Four hundred microlitres of the pooled fractions was added to the beads and incubated on a rotator mixer for 30 min at 4 °C. Remaining at 4 °C, the beads were washed twice in 10 volumes of buffer 1 and twice in 10 volumes of buffer 2 (200 mM KCl, 20 mM HEPES KOH (pH 7.9), 1% Triton X-100, 20 U/ml SUPERase•In, and cOmplete EDTA-free Protease Inhibitor Cocktail). Bound Flag–MCP was eluted from beads with 30 μl of 150 ng/μl 3×Flag peptide (Sigma-Aldrich) on a rotator mixer for 30 min at 4 °C. The eluents were precipitated with TCA, digested with trypsin and labelled with tandem mass tags to allow for quantitative comparisons between six total samples (three control and three test samples). Peptides were analysed by liquid chromatography–tandem mass spectrometry using an Orbitrap Elite (Thermo Fisher) coupled with a NanoAcquity UPLC system (Waters). Peptides were identified using SEQUEST and data analysed using PEAKS Studio (Bioinformatics Solutions).

Experimental design and reproducibility. No statistical methods were used to predetermine sample size. Growth-curve cultures were randomized by permutation of strain placement on 96-well plates across experiments. Edge effects were not significant within the time span that measurements were taken. The investigators were not blinded to allocation during experiments and outcome assessment. RNA-seq results for biological replicates correlated well (log-phase culture, $R^2 = 0.98$ (mRNA, $n = 5,652$); saturated culture, $R^2 = 0.88$ (mRNA, $n = 5,762$) and 0.78 (stable introns, $n = 30$)).

Reporting summary. Further information on research design is available in the Nature Research Reporting Summary linked to this paper.

Data availability

Sequencing data and the processed data for each gene and intron are available at the Gene Expression Omnibus (http://www.ncbi.nlm.nih.gov/geo) under accession number GSE121765. For gel source data, see Supplementary Fig. 1. All other data are available from the corresponding author upon reasonable request.

46. Weinberg, D. E. et al. Improved ribosome-footprint and mRNA measurements provide insights into dynamics and regulation of yeast translation. *Cell Reports* **14**, 1787–1799 (2016).
47. Harju, S., Fedosyuk, H. & Peterson, K. R. Rapid isolation of yeast genomic DNA: Bust 'n Grab. *BMC Biotechnol.* **4**, 8 (2004).
48. Subtelny, A. O., Eichhorn, S. W., Chen, G. R., Sive, H. & Bartel, D. P. Poly(A)-tail profiling reveals an embryonic switch in translational control. *Nature* **508**, 66–71 (2014).
49. Martin, M. Cutadapt removes adapter sequences from high-throughput sequencing reads. *EMBnet J.* **17**, 10–12 (2011).
50. Dobin, A. et al. STAR: ultrafast universal RNA-seq aligner. *Bioinformatics* **29**, 15–21 (2013).
51. Robinson, J. T. et al. Integrative genomics viewer. *Nat. Biotechnol.* **29**, 24–26 (2011).
52. Thorvaldsdóttir, H., Robinson, J. T. & Mesirov, J. P. Integrative Genomics Viewer (IGV): high-performance genomics data visualization and exploration. *Brief. Bioinform.* **14**, 178–192 (2013).
53. Bailey, T. L. et al. MEME SUITE: tools for motif discovery and searching. *Nucleic Acids Res.* **37**, W202–W208 (2009).
54. Wu, X. & Bartel, D. P. kpLogo: positional *k*-mer analysis reveals hidden specificity in biological sequences. *Nucleic Acids Res.* **45**, W534–W538 (2017).
55. Pall, G. S., Codony-Servat, C., Byrne, J., Ritchie, L. & Hamilton, A. Carbodiimide-mediated cross-linking of RNA to nylon membranes improves the detection of siRNA, miRNA and piRNA by northern blot. *Nucleic Acids Res.* **35**, e60 (2007).
56. Chee, M. K. & Haase, S. B. New and redesigned pRS plasmid shuttle vectors for genetic manipulation of *Saccharomyces cerevisiae*. *G3 (Bethesda)* **2**, 515–526 (2012).
57. Zalatan, J. G. et al. Engineering complex synthetic transcriptional programs with CRISPR RNA scaffolds. *Cell* **160**, 339–350 (2015).
58. McFarlane, E. S. Ribonuclease activity during G1 arrest of the yeast *Saccharomyces cerevisiae*. *Arch. Microbiol.* **124**, 243–247 (1980).
59. Wan, R., Yan, C., Bai, R., Lei, J. & Shi, Y. Structure of an intron lariat spliceosome from *Saccharomyces cerevisiae*. *Cell* **171**, 120–132.e112 (2017).

Extended Data Fig. 1 | RNA-seq coverage across the branch point and to the 3′SS of the *ECM33* intron. The pileup of reads mapping to the 61-nucleotide region centred on the *ECM33* branch point, replotted from Fig. 1b, is shown (red, top). The position of the branch point (closed circle with flanking dashed lines) is indicated on the intron (thick grey line) and relative to the 3′ exon (grey box). Bottom, all reads mapping uniquely to this region are shown (thin grey lines). Reads mapping across the exon–exon junction are coloured blue in the region of the excised intron and are shown above the other reads. Mismatched nucleotides within reads are indicated with coloured bars, with the colour of the bar indicating the identity of the mismatch. Terminal untemplated nucleotides have been clipped from reads.
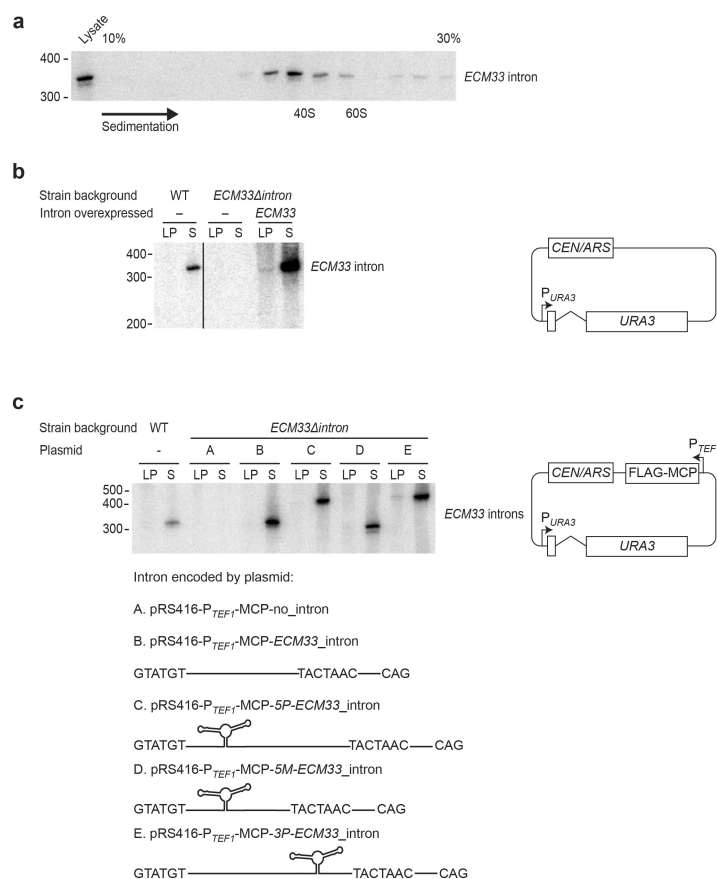
Extended Data Fig. 2 | Stable-intron sedimentation and expression constructs for pull-down and mass spectrometry. a, Co-sedimentation of the *ECM33* stable intron with large ribonucleoprotein complexes. Cleared lysate from a saturated yeast culture was fractionated by sedimentation into a 10–30% sucrose gradient, and RNA was extracted from each fraction. An RNA blot that resolved 25% of the RNA from each fraction and was probed for the *ECM33* intron is shown. Fractions are oriented with increasing sedimentation from left to right. RNA was also extracted from 12.5% of the total lysate before sedimentation, of which 50% was loaded for comparison (left lane). The sedimentation of 40S and 60S complexes is marked on the basis of the location of ribosome subunits. Migration of markers with lengths indicated (in nucleotides) is shown on the left. *n* = 6 biological replicates. **b**, Behaviour of stable introns ectopically expressed from the *URA3* gene. An RNA blot probed for the *ECM33* intron after resolving total RNA from cultures expressing the *ECM33* intron from the endogenous *ECM33* locus (WT, left lanes), cultures from a strain in which the intron had been deleted (*ECM33Δintron*, middle lanes) and cultures of this deletion strain

ectopically expressing the *ECM33* intron spliced from the plasmid-borne *URA3* reporter gene (right lanes) is shown. pRS416-ECM33_intron plasmid shown on right; P$_{URA3}$, *URA3* promoter; *CEN/ARS* (centromere/ autonomously replicating sequence), low-copy origin of replication. Interior lanes that were not relevant to this experiment were removed from this image (vertical line). Otherwise, this panel is as in Fig. 1c. *n* = 4 biological replicates. **c**, Behaviour of stable introns with MS2 hairpins inserted to be used as affinity tags for pull-downs. Five different plasmids with a common backbone (right; P$_{TEF1}$, *TEF1* promoter; FLAG–MCP, coding region of Flag-tagged MS2 coat protein) each expressed *URA3* with a different variant of the *ECM33* intron (variants A–E, schematized below). These plasmids were each expressed in the strain that lacked an endogenous *ECM33* intron (*ECM33Δintron*). The RNA blot resolved total RNA from the indicated cultures and was probed for a sequence common to the intron variants; otherwise, as in Fig. 1c. The 2 × MS2 hairpin region is 90 nucleotides long, and the expected linear-intron sizes were: A, no intron; B, 330 nucleotides; C, 420 nucleotides; D, 300 nucleotides; and E, 420 nucleotides. *n* ≥ 2 biological replicates.
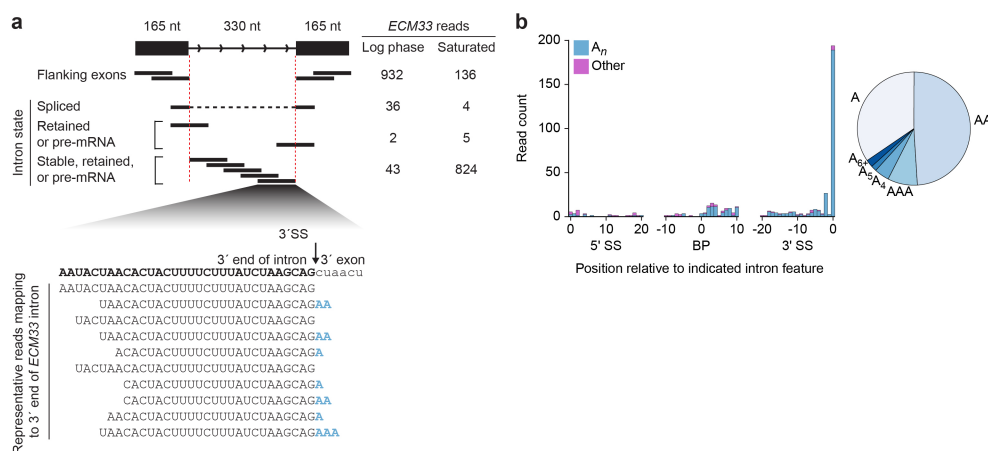
**Extended Data Fig. 3 | Stable introns have oligoadenylate tails.**
a, Example of RNA-seq support for intron accumulation and terminal adenylylation. The diagram (top, left) classifies the RNA-seq reads that derive from the possible intron states of *ECM33* transcripts (black lines, reads; red dashed lines, intron boundaries). Read counts from log-phase and saturated cultures (normalized for library depth) are listed for each class of reads (top, right). For convenient comparison to intron accumulation, exon reads are only counted if they map within 165 nucleotides of either splice site (thereby encompassing 330 nucleotides, the length of the intron). The alignment (bottom) shows representative reads mapping to the intron 3′ terminus, aligned below the sequence of the 3′ intron–exon junction. Many of these reads had untemplated terminal adenosine residues (blue). **b**, Composition of untemplated tailing nucleotides observed in a saturated culture. Reads that had at least one terminal untemplated nucleotide after trimming the 3′ adaptor sequence were collected, and the position of this tail was annotated as that of the last templated nucleotide. Counts of reads with tails added at positions 0 to +20 relative to the 5′SS, −10 to +10 relative to the branch point, and −20 to 0 relative to the 3′SS are plotted, binning counts for tails of only adenosines (A_n, teal) separately from those of all other tails (other, purple). For A_n tails that map to the 3′-terminal nucleotide of introns, the fraction with each indicated length is plotted (right). The relative abundance of A_n at positions −2 and −1 relative to the 3′SS was ambiguous because most introns have an adenosine at position −1 (3′SS consensus sequence, YAG), which causes tails of length n at position −1 to be indistinguishable from tails of length $n + 1$ at position −2.
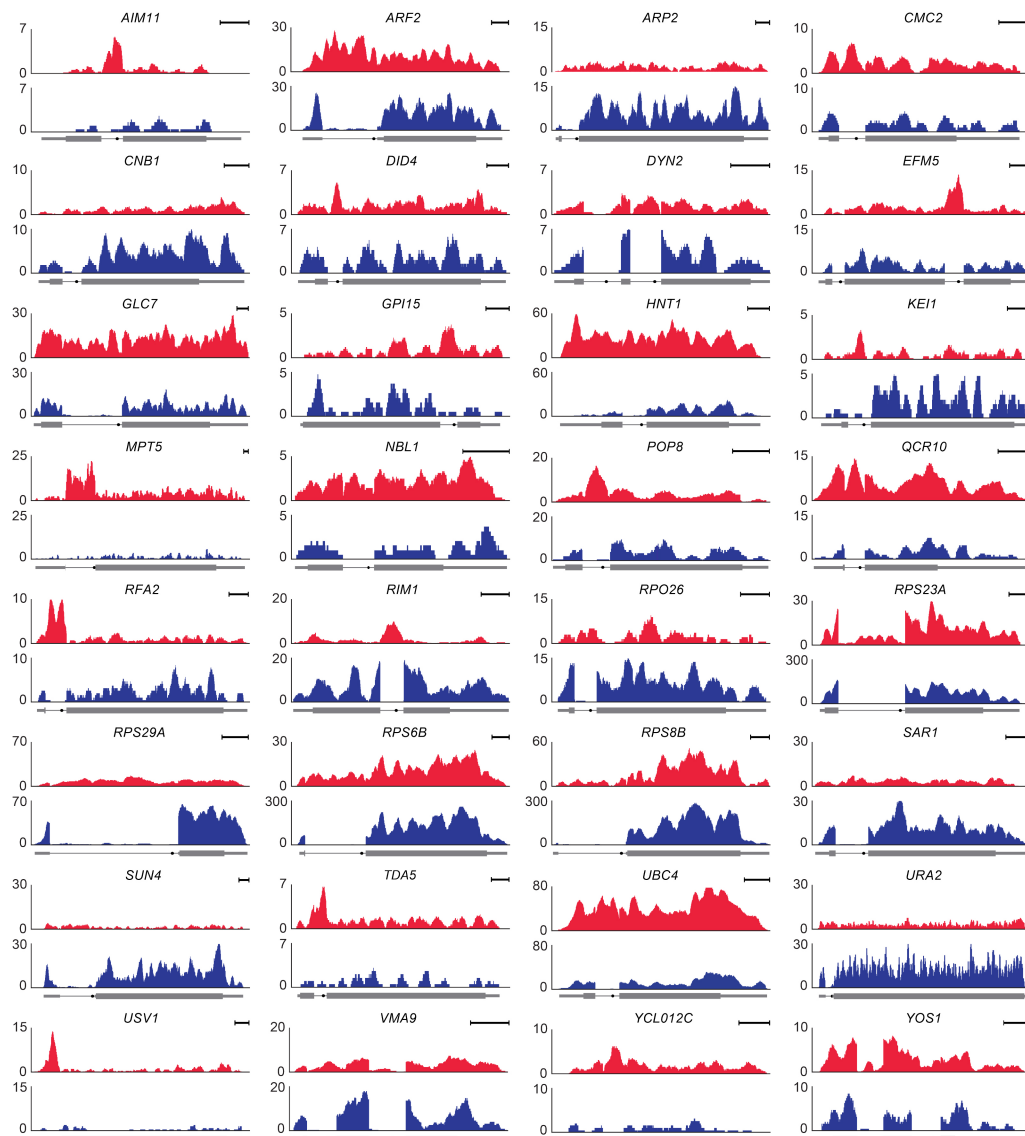
Extended Data Fig. 4 | RNA-seq profiles of genes with stable introns. Profiles from the stable-intron-inducing condition (red) and log-phase culture (blue) are shown for the indicated 32 genes with confidently identified stable introns not already depicted in Fig. 1. For all but four of these, the profile of the stable-intron-inducing condition is from RNA-seq of the saturated-liquid sample. The four exceptions were not confidently identified in saturated liquid (Extended Data Table 2); for these, the profile of the stable-intron-inducing condition is from either the rapamycin-treated sample (*TDA5* and *YOS1*) or the saturated lawn (*RPO26* and *RPS8B*). Scale bars, 100 nucleotides. Otherwise, this panel is as in Fig. 1a.
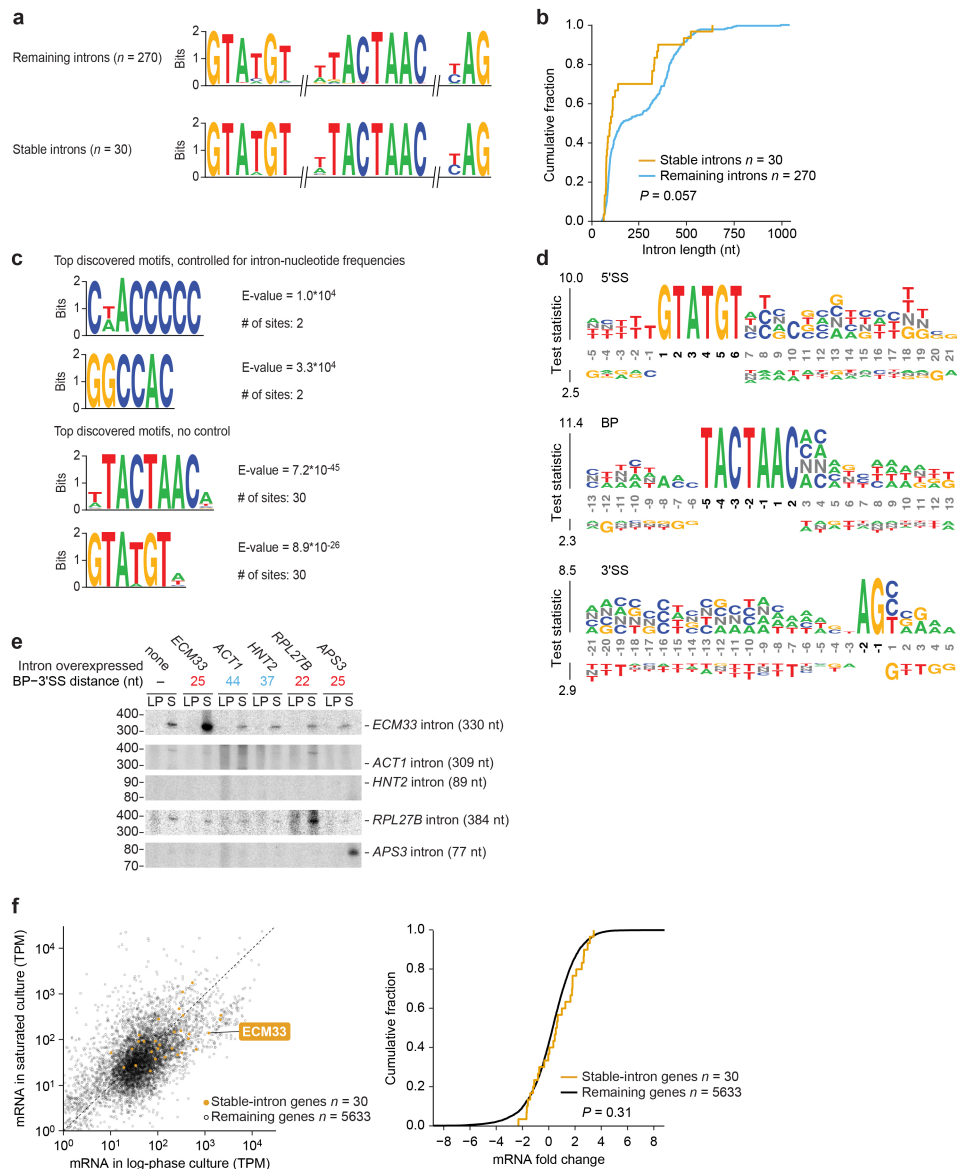
Extended Data Fig. 5 | Stable introns are indistinguishable from other introns in many respects. a, Similar splicing motifs compared to other introns. Information-content logos of splicing motifs (6-mer 5′SS, 8-mer branch point and 3-mer 3′SS) for stable introns (bottom) and other introns (top) are plotted. **b**, Similar length distribution compared to other introns. Cumulative distributions of intron lengths are plotted ($P = 0.057$, two-tailed Kolmogorov–Smirnov test). **c**, No significantly enriched motifs within stable introns. Stable-intron sequence motifs discovered by MEME[53] are plotted, either controlling for k-mer frequencies of non-stable introns (top) or without controlling (bottom). No significant motifs were discovered in stable introns when $k \geq 6$. The motifs discovered without controlling for k-mer frequencies matched the canonical branch point and 5′SS motifs (see **a**). Branch point and 5′SS motifs were also the only significantly enriched motifs discovered when $k \leq 5$. **d**, No enriched positional k-mer motifs detected by kpLogo[54] in stable introns. The most enriched k-mers at positions relative to 5′SS (top), branch point (middle), and 3′SS (bottom) are plotted, comparing stable introns to unstable introns. Stacked nucleotides at a position represent the most significant motif starting at that position. The height is scaled relative to the significance of the motif, as determined by the one-sided binomial test statistic (y axes). Black numbers indicate invariant nucleotides occurring >95% of the time at the position. No k-mers were significantly enriched

when using a Bonferroni-corrected P of 0.01. **e**, Support for a role of branch point–3′SS distance in specifying stable-intron formation. The indicated introns were ectopically expressed from the *URA3* splicing construct (Extended Data Fig. 2b). Results are shown from an RNA blot that resolved total RNA from cultures overexpressing the indicated introns and was probed for the indicated introns (length of excised intron in parentheses). The *ECM33* and *RPL27B* introns were probed sequentially, and then the *ACT1*, *HNT2* and *APS3* introns were probed concurrently. *ACT1* probe was validated on synthetic transcripts resembling the *ACT1* intron, which were produced by in vitro transcription (not shown). Migration of markers with lengths (in nucleotides) indicated is at the left. $n \geq 2$ biological replicates. **f**, Expression of mRNAs from genes containing stable introns. Left, relationship between the expression in log-phase and saturated cultures (expression cutoff, 1 TPM in both samples). Points for genes containing stable introns are indicated (orange), and the point for *ECM33* is labelled. Right, comparison of the expression results of genes with stable introns to those of the remaining genes. The cumulative distributions of fold changes in expression (expressed as $\log_2$(mRNA in log-phase culture/mRNA in saturated culture)) observed between log-phase and saturated cultures are plotted, which shows no significant difference between stable-intron genes and other genes ($P = 0.31$ two-tailed Kolmogorov–Smirnov test).
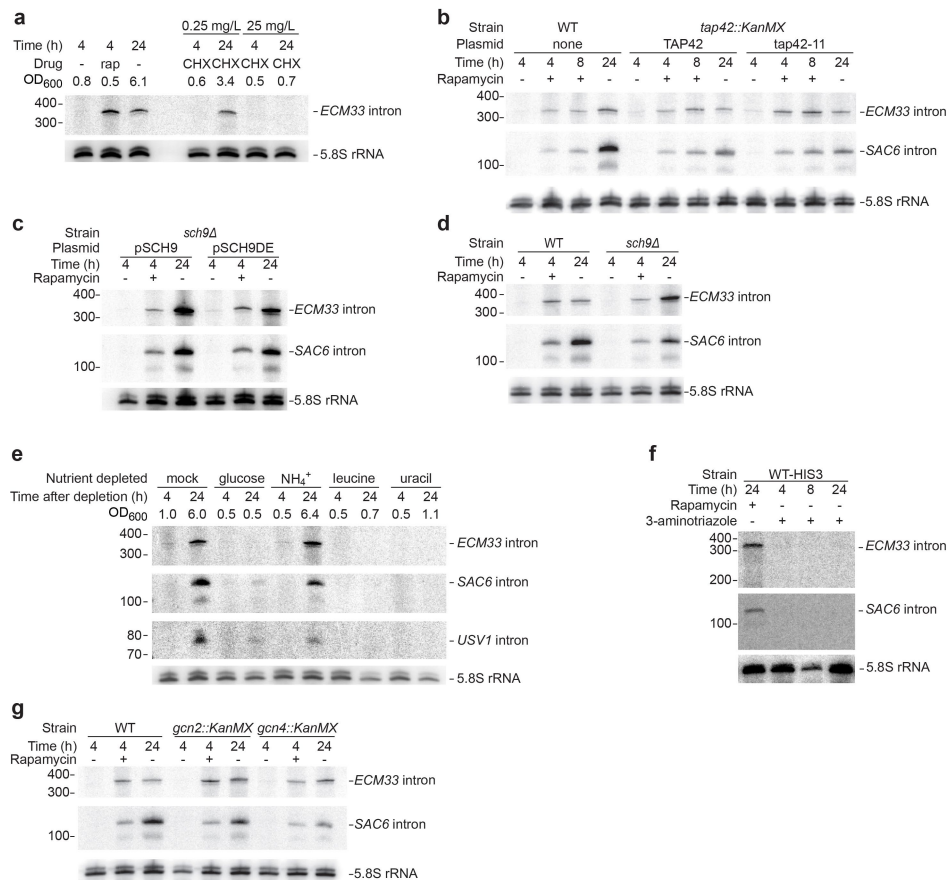
Extended Data Fig. 6 | Assessing aspects of TORC1 regulation on stable-intron expression. a, Inability of TORC1-independent inhibition of protein synthesis to prematurely induce stable-intron accumulation. The left lanes show a replicate of Fig. 3b, and the right lanes show results after treatment with either low (0.25 mg l^{-1}) or high (25 mg l^{-1}) concentrations of cycloheximide. As indicated by OD$_{600\,nm}$ at collection, the mild cycloheximide treatment allowed the culture to reach an OD$_{600\,nm}$ of 3.4 after 24 h, which was equivalent to the OD$_{600\,nm}$ of 10 h without cycloheximide (Fig. 3a). **b**, Dispensability of TORC1-responsive Tap42 for stable-intron formation. Samples were grown at 25 °C owing to temperature sensitivity of the *tap42-11* allele. Additionally, owing to slower growth at 25 °C, the duration of pre-growth was extended to 5.5 h before reseeding in medium with (+) or without (−) rapamycin, such that the change in OD$_{600\,nm}$ of the pre-growth sample matched that of wild-type cultures grown at 30 °C for 4 h. Otherwise, this panel is as in Fig. 3b. *n* = 2 biological replicates. **c**, Dispensability of TORC1-sensitive Sch9 for stable-intron formation. Samples were grown in SC–Trp medium to maintain plasmids that expressed either TORC1-sensitive (pSCH9) or TORC1-insensitive (pSCH9DE) Sch9 protein. Because of the slower growth of the *sch9Δ pRS414::SCH9* and *sch9Δ pRS414::SCH9DE* strains (possibly owing to the requisite SC–Trp medium) the duration of pre-growth was extended to 5 h, such that the change in OD$_{600\,nm}$ of the pre-growth sample matched that of wild-type cultures grown for 4 h. Otherwise, this panel is as in Fig. 3b. *n* = 3 biological replicates. **d**, Dispensability of Sch9

for stable-intron formation. The left lanes show a replicate of Fig. 3b, and the right lanes show the same experiments performed in the *sch9Δ* strain. *n* = 2 biological replicates (*sch9Δ* samples). **e**, Inability of acute deprivation of select nutrients to induce accumulation of stable introns. To prevent contamination of starting cultures with stable introns contributed by inoculum, cultures were seeded at OD$_{600\,nm}$ = 0.2 from an overnight culture that was allowed to grow to mid-log phase, collected by vacuum filtration, washed in water and resuspended in fresh medium that lacked the indicated nutrients. Cultures were collected after the indicated times and analysed as in Fig. 1c, except the RNA blot was sequentially re-probed for the *ECM33*, *SAC6* and *USV1* introns. As indicated by OD$_{600\,nm}$ at collection, the sample deprived of ammonium sulfate (the main source of nitrogen) was still able to reach a high density after 24 h. *n* ≥ 2 biological replicates. **f**, Inability of the general amino acid control response to induce stable introns. Early-log-phase cultures were treated with either 100 nM rapamycin or 50 mM 3-aminotriazole for the indicated times. Cultures were grown in SC–His to force inhibition of histidine biosynthesis by 3-aminotriazole. Cultures treated with 3-aminotriazole for 24 h did not reach a density sufficient to induce stable-intron accumulation by approaching saturated growth. **g**, Stable-intron accumulation despite inability to induce the general amino acid control pathway. The left lanes show a replicate of Fig. 3b, and the middle and right lanes show the same experiments performed in *gcn2Δ* and *gcn4Δ* strains, respectively.
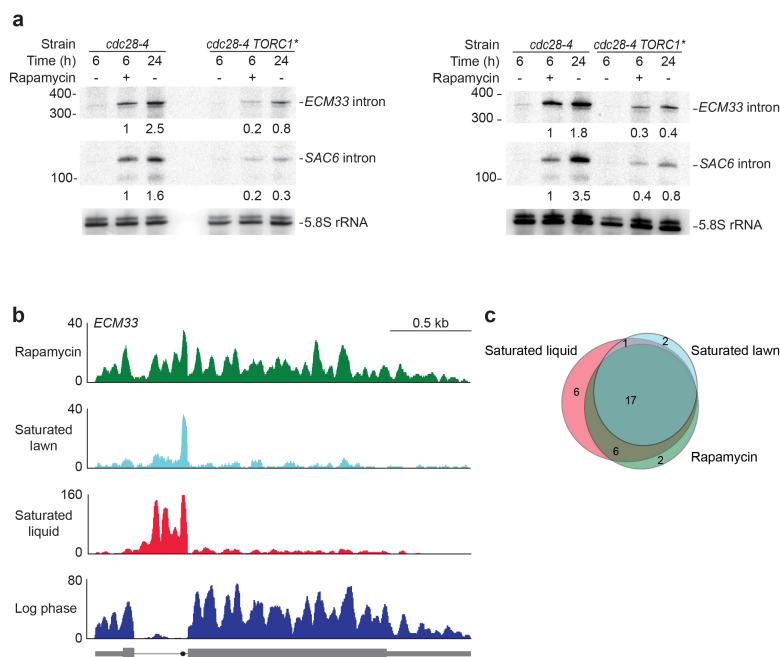
Extended Data Fig. 7 | The influence of hyperactive TORC1 on stable-intron formation. a, The left and right panels are biological replicates comparing *ECM33* and *SAC6* intron levels in a strain with hyperactive TORC1 (TORC1*) to those in a strain-background control (*cdc28-4*). Growth conditions were as described for these strains[31]. Overexpression of Sfp1 was induced 1 h before treatment with rapamycin (or no treatment). Owing to the decreased growth rate of these strains in the requisite conditions, samples with and without rapamycin were collected after 6 h of treatment rather than after 4 h of treatment. Numbers below the *ECM33* and *SAC6* intron blots indicate the level of each intron normalized to the

level in the *cdc28-4* rapamycin-treated samples, after first normalizing all lanes to the 5.8S rRNA loading control (set to 1). **b**, Accumulation of the *ECM33* intron in rapamycin-treated, saturated-lawn and saturated-liquid cultures, detected using RNA-seq. Results showing accumulation of this intron in saturated-liquid culture but not log-phase culture are from a different biological replicate than that shown in Fig. 1a, b; otherwise, this panel is as in Fig. 1a. Rapamycin results are re-plotted from Fig. 3d (4 h). **c**, Overlap between stable introns identified in saturated-liquid, saturated-lawn and rapamycin-treated cultures.
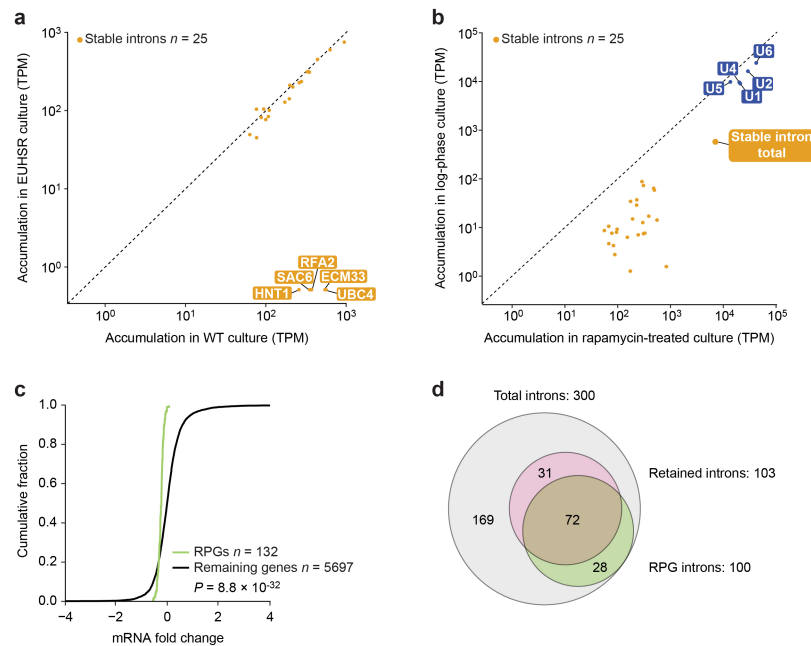
Extended Data Fig. 8 | Evidence for spliceosome sequestration and control of ribosome production by stable introns. a, No evidence for compensatory stable-intron expression after genomic deletion of five stable introns. The scatter plot shows the relationship between intron accumulation in rapamycin-treated, wild-type culture and in rapamycin-treated, EUHSR culture, focusing on the 25 stable introns detected after rapamycin treatment (Extended Data Table 2). The dashed line is placed at $x = y$. Stable introns are indicated (closed orange circles). Points for introns deleted from the EUHSR genome (*ECM33*, *UBC4*, *HNT1*, *SAC6* and *RFA2*) are labelled. All introns were pseudocounted at 0.5 TPM. **b**, Aggregate stable-intron accumulation approaching that of spliceosomal RNAs. Levels of stable introns and spliceosomal RNAs (labelled closed blue circles) are plotted, comparing levels in log-phase, wild-type culture to those in rapamycin-treated, wild-type culture. The aggregate stable-intron abundance (closed orange circle, stable intron total) is also plotted. Much of the apparent accumulation observed in log-phase culture was attributable to reads from a few highly transcribed stable-intron genes (for example, *RPS29A*, which has an intron:mRNA TPM ratio of 107:2,030 in log phase compared to 289:319 in saturated culture). Otherwise, as in **a**.

c, Reduced expression of mRNA of ribosomal protein genes (RPGs) when overexpressing a stable intron in rapamycin-treated EUHSR culture. The cumulative distributions of fold changes in mRNA expression (expressed as $\log_2$(mRNA in EUHSR expressing *ECM33* intron/mRNA in EUHSR expressing *ACT1* intron)) observed between an EUHSR culture with stable-intron (*ECM33*) ectopic expression and an EUHSR culture with control-intron (*ACT1*) ectopic expression are plotted. The distribution of changes for mRNAs of RPGs (green) differed from that of other genes (black), with generally lower expression of RPGs in the culture that overexpresses the stable intron ($P = 8.8 \times 10^{-32}$, one-tailed Kolmogorov–Smirnov test; expression cutoff, 1 TPM in both samples). **d**, Less efficient splicing—as detected by increased intron retention—when overexpressing a stable intron in rapamycin-treated, EUHSR culture. When analysing the dataset in **c**, 103 genes had significantly more intron retention when ectopically expressing the stable intron compared to when expressing the control intron (MISO, Bayes factor > 100). The Venn diagram shows the overlap between these genes with increased intron retention and intron-containing RPGs ($P = 3.9 \times 10^{-22}$, hypergeometric test).

Extended Data Table 1 | Proteins associated with stable introns

Protein name	Enrichment values							Mean control	Mean test	Fold difference
	Control 1	Control 2	Control 3	Test 1	Test 2	Test 3		Mean control	Mean test	Fold difference
Prp9	0.11	1.00	0.57	4.84	6.34	4.83		0.56	5.34	9.54
Hsh49	0.60	1.00	1.20	5.67	5.15	5.24		0.93	5.35	5.74
Cef1	0.93	1.00	0.99	3.45	6.04	5.79		0.97	5.09	5.23
Rse1	0.66	1.00	0.90	3.17	4.16	5.80		0.85	4.38	5.13
Bud31	0.68	1.00	0.96	3.96	3.96	4.16		0.88	4.03	4.58
Prp45	0.88	1.00	0.71	3.12	3.77	3.86		0.86	3.58	4.15
Prp19	0.87	1.00	1.05	3.28	4.03	4.20		0.97	3.84	3.94
Brr2	0.78	1.00	0.69	2.22	3.21	3.66		0.82	3.03	3.68
Prp8	0.75	1.00	0.73	2.00	2.63	3.46		0.83	2.70	3.26
Smb1	0.67	1.00	1.10	2.49	2.80	2.69		0.92	2.66	2.88

Results are shown for the ten proteins that were consistently enriched $\geq$ 2-fold in stable-intron pull-down eluates. Three control samples without a tagged intron and three test samples with unique tagged introns (Extended Data Fig. 2, Supplementary Table 5) were simultaneously analysed by quantitative mass spectrometry. These ten proteins were the only proteins that were enriched $\geq$ 2-fold in each of the 9 possible pairwise comparisons between test and control samples. The identities of these proteins were consistent with the excised and debranched introns being part of a complex that resembles the ILS complex, in that all ten are known components of the ILS identified through biochemical studies[23], and most (all but Brr2, Hsh49, Prp9 and Rse1) have also been identified in a cryo-EM structure of the ILS complex[59]. Moreover, several early spliceosome components (Luc7, Prp3, Snp1 and Snu13) as well as an essential disassembly factor (Prp43) were detected in all samples but not enriched in tagged-intron eluates. The observation that the intron did not co-purify with exonic sequences also helped to rule out the possibility that it was part of a complex that resembled earlier spliceosomal complexes. Enrichment values were those reported by PEAKS Studio, which are reported relative to values of control 2.

Extended Data Table 2 | Stable introns of *S. cerevisiae*

Stable intron	Liquid	Rapamycin	Lawn	BP-3'SS distance (nt)	Intron length (nt)	Description of gene function
AIM11	●		●	20	75	Protein of unknown function
ARF2	●	●	●	18	332	ADP-ribosylation factor
ARP2	●	●		15	123	Essential component of the Arp2/3 complex
CMC2	●	●	●	29	85	Protein involved in respiratory chain complex assembly or maintenance
CNB1	●	●		19	76	Calcineurin B
DID4	●			23	68	Class E Vps protein of the ESCRT-III complex
DYN2_2	●			17	80	Cytoplasmic light chain dynein, microtubule motor protein
ECM33	●	●	●	25	330	GPI-anchored protein of unknown function
EFM5_2	●	●	●	25	93	S-adenosylmethionine-dependent lysine methyltransferase
GLC7	●	●	●	31	525	Type 1 S/T protein phosphatase (PP1) catalytic subunit
GPI15	●	●		14	74	Protein involved in the synthesis of GlcNAc-PI
HNT1	●	●		23	111	Adenosine 5'-monophosphoramidase
KEI1	●			31	101	Component of inositol phosphorylceramide (IPC) synthase
MPT5	●	●	●	25	640	mRNA-binding protein of the PUF family
NBL1	●	●	●	12	67	Subunit of the conserved chromosomal passenger complex (CPC)
POP8	●	●	●	20	75	Subunit of both RNase MRP and nuclear RNase P
QCR10	●			15	63	Subunit of the ubiqunol-cytochrome c oxidoreductase complex
RFA2	●	●	●	24	108	Subunit of heterotrimeric Replication Protein A (RPA)
RIM1	●	●	●	26	83	ssDNA-binding protein essential for mitochondrial genome maintenance
RPO26			●	21	76	RNA polymerase subunit ABC23
RPS23A	●			23	319	Ribosomal protein 28 (rp28) of the small (40S) ribosomal subunit
RPS29A	●	●		22	488	Protein component of the small (40S) ribosomal subunit
RPS6B	●	●	●	23	352	Protein component of the small (40S) ribosomal subunit
RPS8B			●	24	360	Protein component of the small (40S) ribosomal subunit
SAC6	●	●	●	20	111	Fimbrin, actin-bundling protein
SAR1	●	●		19	139	ARF family GTPase
SUN4	●			22	346	Cell wall protein related to glucanases
TDA5		●		19	71	Protein of unknown function
UBC4	●	●	●	26	95	Ubiquitin-conjugating enzyme (E2)
URA2	●	●	●	22	320	Bifunctional carbamoylphosphate synthetase/aspartate transcarbamylase
USV1	●	●	●	24	75	Putative transcription factor containing a C2H2 zinc finger
VMA9_1	●	●	●	22	77	Vacuolar H+ ATPase subunit e of the V-ATPase V0 subcomplex
YCL012C	●	●	●	13	65	Protein of unknown function
YOS1_2		●		24	111	Integral membrane protein required for ER to Golgi transport

If a host gene has two introns, a suffix specifies whether the first or second intron is stabilized (_1 and _2, respectively). Description of gene function is from YeastMine (https://yeastmine.yeastgenome.org/). Liquid, saturated-liquid sample; lawn, saturated-lawn sample; rapamycin, rapamycin-treated sample.

Corresponding author(s):   David Bartel

Reporting Summary

Nature Research wishes to improve the reproducibility of the work that we publish. This form provides structure for consistency and transparency in reporting. For further information on Nature Research policies, see Authors & Referees and the Editorial Policy Checklist.

Statistical parameters

When statistical analyses are reported, confirm that the following items are present in the relevant location (e.g. figure legend, table legend, main text, or Methods section).

n/a	Confirmed	
☐	☒	The exact sample size (n) for each experimental group/condition, given as a discrete number and unit of measurement
☐	☒	An indication of whether measurements were taken from distinct samples or whether the same sample was measured repeatedly
☐	☒	The statistical test(s) used AND whether they are one- or two-sided *Only common tests should be described solely by name; describe more complex techniques in the Methods section.*
☒	☐	A description of all covariates tested
☐	☒	A description of any assumptions or corrections, such as tests of normality and adjustment for multiple comparisons
☐	☒	A full description of the statistics including central tendency (e.g. means) or other basic estimates (e.g. regression coefficient) AND variation (e.g. standard deviation) or associated estimates of uncertainty (e.g. confidence intervals)
☐	☒	For null hypothesis testing, the test statistic (e.g. F, t, r) with confidence intervals, effect sizes, degrees of freedom and P value noted *Give P values as exact values whenever suitable.*
☒	☐	For Bayesian analysis, information on the choice of priors and Markov chain Monte Carlo settings
☒	☐	For hierarchical and complex designs, identification of the appropriate level for tests and full reporting of outcomes
☐	☒	Estimates of effect sizes (e.g. Cohen's d, Pearson's r), indicating how they were calculated
☐	☒	Clearly defined error bars *State explicitly what error bars represent (e.g. SD, SE, CI)*

Our web collection on statistics for biologists may be useful.

Software and code

Policy information about availability of computer code

Data collection	No software was used.
Data analysis	RNA-blot data were analyzed with ImageQuant TL (v8.1.0.0). Growth curves were analyzed with SkanIt (v3.2). RNA-seq data were analyzed with cutadapt (v1.8), STAR (v2.4), and MISO (v0.5.4), and visualized with IGV (v2.3.57).

For manuscripts utilizing custom algorithms or software that are central to the research but not yet described in published literature, software must be made available to editors/reviewers upon request. We strongly encourage code deposition in a community repository (e.g. GitHub). See the Nature Research guidelines for submitting code & software for further information.

Data

Policy information about availability of data

All manuscripts must include a data availability statement. This statement should provide the following information, where applicable:

- Accession codes, unique identifiers, or web links for publicly available datasets
- A list of figures that have associated raw data
- A description of any restrictions on data availability

Sequencing data and the processed data for each gene and intron are available at the Gene Expression Omnibus (http://www.ncbi.nlm.nih.gov/geo) under accession number GSE121765. For gel source data, see Supplementary Figure 1. All other data are available from upon reasonable request.

Field-specific reporting

Please select the best fit for your research. If you are not sure, read the appropriate sections before making your selection.

☒ Life sciences   ☐ Behavioural & social sciences   ☐ Ecological, evolutionary & environmental sciences

For a reference copy of the document with all sections, see nature.com/authors/policies/ReportingSummary-flat.pdf

Life sciences study design

All studies must disclose on these points even when the disclosure is negative.

Sample size	In growth-curve experiments, technical replicates were used for each strain/condition combination, per standard practice. Variance observed between biological replicates showed that three were sufficient for growth curves and one was sufficient for RNA-seq.
Data exclusions	In growth-curve experiments, single wells were excluded if artifactual spikes in absorbance attributable to bubbles or condensation were observed. Results for a replicate were excluded if more than one well was censored.
Replication	RNA-seq results for biological replicates correlated well (log-phase culture, Pearson R2 = 0.98 [mRNA, n = 5652]; saturated culture, Pearson R2 = 0.88 [mRNA, n = 5762] and 0.78 [stable introns, n = 30]). Growth curves were each performed using at least 3 biological replicates.
Randomization	Growth-curve cultures were randomized by permutation of strain placement on 96-well plates across experiments.
Blinding	LC/MS: peak selection and data analysis were done blindly by the staff of the metabolic profiling facility, without knowledge of conditions.

Reporting for specific materials, systems and methods

Materials & experimental systems

n/a	Involved in the study
☐	☒ Unique biological materials
☒	☐ Antibodies
☐	☒ Eukaryotic cell lines
☒	☐ Palaeontology
☒	☐ Animals and other organisms
☒	☐ Human research participants

Methods

n/a	Involved in the study
☒	☐ ChIP-seq
☒	☐ Flow cytometry
☒	☐ MRI-based neuroimaging

Unique biological materials

Policy information about availability of materials

Obtaining unique materials	Unique yeast strains and plasmids are available upon request from the authors and Addgene, respectively.

Eukaryotic cell lines

Policy information about cell lines

Cell line source(s)	Yeast strains not unique to this study are common strains (BY4741, W303a), were requested from labs of origin per standard practice, or were obtained commercially (yeast knock out collection, Horizon Discovery).
Authentication	ORF deletions, intron deletions, and BP manipulations were authenticated by amplification and Sanger sequencing across loci of interest.
Mycoplasma contamination	Because our eukaryotic cell lines were all yeasts, no mycoplasma testing was performed.
Commonly misidentified lines (See ICLAC register)	No commonly misidentified cell lines were used.